WBMsed, a distributed global-scale riverine sediment flux model: Model description and validation

Sagy Cohen [a,*], Albert J. Kettner [a], James P.M. Syvitski [a], Balázs M. Fekete [b]

[a] Community Surface Dynamics Modeling System, Institute of Arctic and Alpine Research, University of Colorado, Boulder, CO 80309, USA
[b] CUNY Environmental CrossRoads Initiative, NOAA-CREST Center, The City College of New York, City University of New York, NY 10031, USA

ARTICLE INFO

ABSTRACT

Quantifying continental sediment flux is a fundamental goal of earth-system science. Ongoing measurements of riverine-suspended sediment fluxes to the oceans are limited ($<10\%$ of rivers) and intrabasin measurements are even scarcer. Numerical models provide a useful bridge to this measurement gap and offer insight to past and future trends in response to human and environmental changes. BQART is a global empirical model that calculates long-term suspended sediment loads. The Psi statistical model accounts for intra- and interannual variability in these BQART sediment flux predictions. Here BQART and Psi are compiled as a new module of the WBMplus global daily water balance/transport model, a central component in the FrAMES hydrological–biogeochemical modeling scheme. The resulting model (WBMsed) simulates spatially and temporally explicit (pixel scale and daily) sediment fluxes over continental Earth. We test WBMsed predictions with (1) observed sediment loads at 95 river mouths and to the original BQART predictions for these rivers, and (2) 11 years of daily sediment flux observations of 11 USGS stations. The results show that WBMsed captures the multiyear average, interannual and intraannual trends but considerably over- and underpredict daily fluxes for extreme discharge periods. These over- and underpredictions are mainly driven by respective mispredictions of water discharge fluxes. Future improvements to WBMsed to address these limitations are provided.

© 2011 Elsevier Ltd. All rights reserved.

1. Introduction

Global sediment dynamics is a key feature of planet geology, biogeochemistry (e.g., landscape evolution, carbon cycle; Syvitski and Milliman, 2007; Vörösmarty et al., 1997a,b), and human-related activities (e.g., water quality, infrastructure; Kettner et al., 2010). Spatially and temporally explicit descriptions of continental sediment fluxes provide a framework for studying a multitude of processes and drivers affecting our environment (e.g., deforestation, climate change, soil production, and erosion; Cohen et al., 2008a, 2009, 2010). Unfortunately sediment measurements are limited. Ongoing sediment fluxes to the oceans are measured for less than 10% of the Earth's rivers (Syvitski et al., 2005b) and intrabasin measurements are even scarcer (Kettner et al., 2010).

Numerical models can fill the gap in sediment dynamic measurements (e.g., Syvitski et al., 2005b; Wilkinson et al., 2009) and offer insight into future and past trends in response to environmental and human changes (e.g., climate change; Kettner and Syvitski, 2009). Simulating global riverine sediment fluxes is a challenging quest as a variety of diverse processes act on the weathering of soil and rock in different parts of the world (Cohen et al., 2010), and its cascade to the coastal oceans or other inland sedimentary basins. Simulating global sediment fluxes become even more challenging when intrabasin predictions are warranted. To avoid simulation discontinuities, a comprehensive global fluvial sediment predictor is desired as river basins cover wide-ranging climatic and geologic zones.

Syvitski and Milliman (2007) compiled a global model (BQART) based on a dimensional analysis of the key operating variables that express the empirical relationship among basin geomorphic (area and relief), hydrologic (discharge), climatic (temperature), geologic (lithology and ice cover), and human (reservoir trapping and soil erosion) characteristics and long-term suspended sediment loads for 66% of the global land surface. The BQART model was trained on a database of 294 river basins (M&S92+; Milliman and Syvitski, 1992) to calculate sediment loads to the oceans and compared to observed sediment loads of 488 rivers (the M&F05 database; Syvitski and Milliman, 2007). With a bias of only 3% and R^2 of 0.95 Syvitski and Milliman (2007) show that the model can be applied successfully (on average within $\pm 38\%$ of the observed fluxes) to a set of very diverse rivers that range across orders of magnitude in area, discharge, and sediment flux. The BQART model was incorporated

Nomenclature

W_s	soil moisture (mm)
E_p	potential evapotranspiration (mm d^{-1})
P_a	precipitation (mm d^{-1})
D_{ws}	soil moisture deficit (mm)
W_c	available water capacity (mm)
α	empirical constant set to 5.0 (dimensionless)
$g(W_s)$	a soil function (dimensionless)
Q_{in}	input flow (m^3 s^{-1})
Q_{out}	released water from the river segment (m^3 s^{-1})
c_1 c_2 c_3	Muskingum coefficients (dimensionless)
$\overline{Qs}$	long-term average suspended sediment load (kg s^{-1})
ω	coefficient of proportionality (dimensionless)
$\overline{Q}$	long-term average water discharge (m^3 s^{-1})
A	upstream contributed area (km^2)
R	maximum relief of upstream area (km)
T	average temperature (°C)
B	a term accounts for geological and human factors (dimensionless)
I	glacial erosion factor (dimensionless)
L	lithology factor (dimensionless)
T_E	reservoirs sediment trapping factor (dimensionless)
E_h	human-influenced soil erosion factor (dimensionless)
Qs	suspended sediment flux (kg s^{-1})
Q	water discharge (m^3 s^{-1})
$\psi_{[i]}$	describes a lognormal random distribution (dimensionless)
$C_{(a)}$	normally distributed annual rating exponent (dimensionless)
E	mean of the $\psi_{[i]}$ lognormal random distribution (dimensionless)
σ	standard deviation of the $\psi_{[i]}$ lognormal random distribution (dimensionless)
$\overrightarrow{F}$	spatially averaged model parameter (parameter dependent)
F_i	a parameter value in a contributing pixel (i) to F_n (parameter-dependent)
P_i	pixel area (km^2)
$\overline{F}$	temporally average model parameter (parameter dependent)

into a basin-outlet model HydroTrend v.3.0 (Kettner and Syvitski, 2008). HydroTrend v.3.0 predicts daily sediment fluxes using the Psi variability model (Morehead et al., 2003) to distribute the BQART long-term average loads.

Although used in intrabasin applications by individually simulating subbasins (i.e., Kettner et al., 2010; McCarney-Castle, 2011), HydroTrend/BQART is a point scale (river mouth) model and therefore cannot explicitly predict riverine flow-path sediment fluxes. To address this limitation, we extend BQART as a spatially distributed global-scale suspended sediment flux model. We compile the BQART and Psi models as a module of the WBMplus global daily water balance/transport model (Wisser et al., 2010a). The WBMplus model was chosen in this regard as it provides a spatially and temporally explicit (pixel-scale and daily, respectively) modular modeling platform that readily includes about half the input datasets needed to operate BQART and Psi.

The new model (termed WBMsed) predictions are validated here by:

(1) A comparison to observed long-term average sediment loads at 95 global river mouths and the original BQART calculations for these rivers.
(2) A comparison to 11 years of daily suspended-sediment flux observations of 11 USGS hydrological stations over the continental United States.

The results show that WBMsed can well predict long-term average sediment flux and can capture intraannual and interannual trends (R^2 of 0.54 for average monthly predictions) but tend to over- and underpredict daily sediment fluxes mainly due to mispredictions of water discharge.

All models described in this paper are freely available through the CSDMS (Community Surface Dynamics Modeling System) model repository (http://csdms.colorado.edu/wiki/Model_download_protal).

2. Modeling architecture

The WBMsed model (Fig. 1) is a spatially and temporally explicit (pixel-scale and daily) implementation of the BQART river-mouth sediment load model (Syvitski and Milliman, 2007). The WBMplus global hydrology model provides a spatially and temporally explicit modeling platform offering many of the desired input datasets. WBM (Vörösmarty et al., 1989) was probably the first hydrological model applied to a global domain. Its most recent version WBMplus is built in the Framework for Aquatic Modeling of the Earth System (FrAMES), a multidisciplinary hydrological/biogeochemical modeling scheme. Perhaps the main difference between WBMplus and comparable large-scale hydrological models is the high degree of flexibility in terms of specifying both computation domains or input data and configuration. For instance, potential evapotransporation calculation alone has nine implementations ranging from a simple air temperature-driven Hamon (1963) function to more complex land cover-dependent approaches (Federer et al., 1996; Vörösmarty et al., 1998). WBM has a demonstrated bias with 5–8 mm/year (Vörösmarty et al., 1998; Fekete et al., 2002) with respect to annual runoff (297 mm/year; Fekete et al., 2002). Numerous studies have shown that the most critical input variable is precipitation (Fekete et al., 2004; Biemans et al., 2009).

The large-scale distributed implementation of BQART in WBMsed is based on the assumption that each point in space (pixel) is a local river mouth (an outlet of its upstream contributing area). WBMsed therefore needs to dynamically calculate the basin-average parameters of BQART (e.g., temperature, discharge, relief) for each pixel. WBMsed, in its current configuration, does not explicitly model sediment transport, which means that it is not a mass conservative sediment model. Following Kettner and Syvitski (2008; the HydroTrend v.3.0 model), WBMsed uses the Psi model (Morehead et al., 2003) to predict a "representative" daily sediment flux based on the long-term average BQART predictions. By representative we mean that the Psi model is used to provide typical instantaneous values to reflect a river draining a similar basin (geography, geology, discharge).

2.1. Core infrastructure

FrAMES is a spatially and temporally explicit multiscale (local through global) hydrological/biogeochemical modeling scheme (Wollheim et al., 2008). It is an ongoing interdisciplinary project
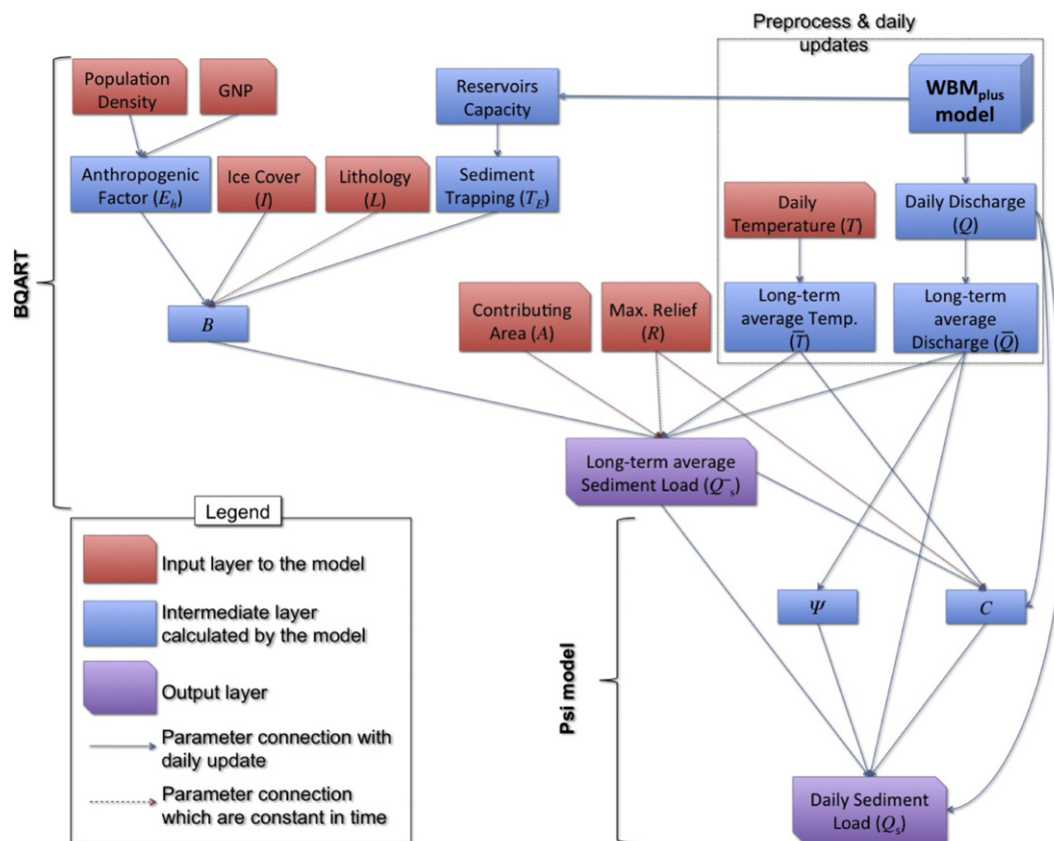
Fig. 1. Schematics of the WBMsed model. WBMsed uses several preexisting WBMplus modules and functions (discharge, reservoirs capacity, and contributing area) and input datasets (temperature, ice cover, and population). The remaining functions and datasets are new.

allowing predictions of changing material flux from major continental rivers in response to changing environmental conditions.

The primary purpose of the FrAMES structure is to separate core modeling components (model I/O, advancing simulation in space and time) from the actual implementation of the simulated processes. FrAMES facilitates user-defined processes on arbitrary topologically linked computational objects, while advancing in time. User-defined processes can request input variables and define computed output variables. Computational objects could map to a vector of grid cells (the typical FrAMES application), points, or polygons. FrAMES offers sequential operations and carries out model I/O at each computational time step to update variables specified as boundary conditions. FrAMES executes the user-defined processes on each computational object, while ensuring that variables defined as output from one process are passed to processes using that variable as input. FrAMES maintains a list of defined variables during model simulations and carries out the input and output as needed.

The topology defined on computational objects allows rudimentary object-to-object operations carried out by FrAMES. Currently, only tree topology is implemented, linking upstream object to the next downstream object. Tree topology provides the basis for the routing operation.

The model modules are defined on single computational objects that are called by FrAMES repeatedly, while advancing in space. FrAMES operates on a list of computational objects that are specified at runtime. These computational objects could represent a series of irregular points, cells of regular or irregular grids, or polygons from a vector coverage. FrAMES handles computational objects in the same manner regardless of their type (from FrAMES perspective any computation domain is just a vector of computational objects). FrAMES offers a limited set of

object-to-object operators (e.g., routing along tree hierarchy or calculating finite differences), which requires object topology (e.g., downstream object for tree hierarchy or the neighbors for finite differences).

2.2. The WBMplus model

The FrAMES enables the water balance/transport model first introduced by Vörösmarty et al. (1989, 1998) and subsequently modified by Wisser et al. (2008, 2010a). At its core the surface water balance of nonirrigated areas is a simple soil moisture budget expressed as

$$dW_s/dt = \begin{cases} -g(W_s)(E_p-P_a) & P_a \le E_p \\ P_a-E_p & E_p < P_a \le D_{ws} \\ D_{ws}-E_p & D_{ws} < P_a \end{cases} \qquad (1)$$

driven by $g(W_s)$ is a unitless soil function

$$g(W_s) = \frac{1-e^{(-\alpha(W_s/W_c))}}{1-e^{-\alpha}}, \qquad (2)$$

and W_s is the soil moisture, E_p is the potential evapotranspiration, P_a is the precipitation (rainfall P_r combined with snowmelt M_s), and D_{ws} is the soil moisture deficit, the difference between available water capacity W_c, which is a soil- and vegetation-dependent variable (specified externally), and the soil moisture. The unitless empirical constant α is set to 5.0 following Vörösmarty et al. (1989).

Potential evopotranspiration can be simulated in various ways by WBMplus, ranging from a simple air temperature drive method to more complex land cover-dependent energy balance calculations (Federer et al., 1996; Vörösmarty et al., 1998). In this

study we used the Hamon equation (Hamon, 1963) that was found to have the least bias in a wide range of climate regions (Federer et al., 1996).

Irrigation is treated separately as a function of irrigated land within each computational grid cell. Wisser et al. (2008, 2010b) provide a detailed description of the calculation of irrigational water demand that ultimately alters the water balance at the grid-cell level. Irrigational water demand is obtained from four sources: (1) small reservoirs, (2) shallow groundwater, (3) nearby rivers, and (4) unsustained deep aquifers.

Small reservoirs are unique to WBMplus and represent small farm ponds that are not captured individually, but as a bulk storage term within each grid cell that contains irrigated land. Small reservoirs are fed by the local runoff generated on the nonirrigated portion of the grid cell, providing freshwater, if available, for irrigation. The mechanism of the small reservoir implementation is discussed in detail in Wisser et al. (2008).

Excess water from surface balance calculation partly forms surface runoff and partly recharges a runoff detention pool representing shallow groundwater aquifers that release water via an exponential decay function. Both the groundwater release and the surface runoff are propagated horizontally along the prescribed river channel.

Flow routing from grid to grid cell following downstream grid-cell tree topology (which only allows conjunctions of grid cells upstream, without splitting to form islands or river deltas) is implemented using the Muskingum-Cunge equation, which is a semi-implicit finite difference scheme to the diffusive wave solution to the St. Venant equations (ignoring the two acceleration terms in the momentum equation) expressed as a linear combination of the input flow from current and previous time steps ($Q_{in\ t-1}$, $Q_{in\ t}$) and the released water from the river segment in the previous time step ($Q_{out\ t-1}$) to calculate new grid-cell outflow:

$$Q_{out\ t} = c_1 Q_{in\ t} + c_2 Q_{in\ t-1} + c_3 Q_{out\ t-1}. \tag{3}$$

The Muskingum coefficients (c_1, c_2, c_3) are traditionally estimated experimentally from discharge records, but their relationships to channel properties are well established. We use a power function approximation of channel geometry $w = ay^b$, expressing the relationship between the river width (w) as a function of flow height (y) from the river bottom. Exponent b dictates the ratio of flow velocity and flood wave celerity. Detailed descriptions are provided in Wisser et al. (2010a).

2.3. The BQART and Psi models

In this global study the BQART model is applied to simulate long-term (30+ years) average suspended sediment loads ($\overline{Qs}$) for each grid cell

$$\overline{Qs} = \omega B \overline{Q}^{0.31} A^{0.5} RT \text{ for } T \geq 2°C, \tag{4a}$$

$$\overline{Qs} = 2\omega B \overline{Q}^{0.31} A^{0.5} R \text{ for } T < 2°C, \tag{4b}$$

where ω is a coefficient of proportionality that equals 0.02 for units of kg s^{-1}, $\overline{Q}$ is the long-term average discharge for each cell, A is the basin upstream contributed area of each cell, R is the relative relief difference between the highest relief of the contributed basin to that cell and the elevation of that particular cell, and T is the average temperature of the upstream contributed area. The B term accounts for important geological and human factors through a series of secondary equations and lookup tables, and includes the effect of glacial erosion processes (I), lithology (L) that expresses the hardness of the rock, and human impact that incorporates both a trapping sediment due to man-made reservoirs (T_E) and a human-influenced soil erosion factor (E_h)

(Syvitski and Milliman, 2007)

$$B = IL(1 - T_E)E_h. \tag{5}$$

The smallest temporal resolution of the WBMplus model is a daily time step. Therefore the Psi Eq. (6) is applied to the long-term sediment flux estimated by applying BQART (Eqs. (4a) and (4b)) to resolve sediment flux on a daily time step. A classic way to calculate daily suspended sediment flux would be by applying $Qs = aQ^{1+b}$ (Ferguson, 1987); however Morehead et al. (2003) developed the Psi equation such that the model is capable of capturing the intra- and interannual variability that natural river systems have

$$\left(\frac{Qs_{[i]}}{\overline{Qs}} \right) = \psi_{[i]} \left(\frac{Q_{[i]}}{\overline{Q}} \right)^{C_{(a)}}, \tag{6}$$

where $Qs_{[i]}$ is the sediment flux for each grid cell, $Q_{[i]}$ is the water discharge leaving the grid cell, $\psi_{[i]}$ describes a lognormal random distribution, [i] is revering to a daily time step, and $C_{(a)}$ is a normally distributed annual rating exponent (Syvitski et al., 2005a) with

$$E(\psi) = 1, \tag{7a}$$

$$\sigma(\psi) = 0.763(0.99995)^{\overline{Q}}, \tag{7b}$$

$$E(C) = 1.4 - 0.025T + 0.00013R + 0.145\ln(\overline{Qs}), \tag{7c}$$

$$\sigma(C) = 0.17 + 0.0000183\overline{Q}, \tag{7d}$$

where E and σ are, respectively, the mean and the standard deviation. Eqs. (7a)–(7d) are reflecting the different variability behavior of various sizes of river systems, where large rivers with high discharges tend to have less intraannual variability in sediment flux than smaller systems (Morehead et al., 2003).

2.4. The WBMsed model

Of the BQART and Psi input parameters simulated by WBMsed, three are temporally static (Eqs. (4a), (4b), and (5)): drainage area (A), maximum relief (R), and lithology factor (L). Area is calculated by summation of pixels sizes upstream. Pixel size is calculated with the WBMplus *MFModelGetArea* function where a drainage network input defines the stream flow routing. Maximum relief is an input dataset calculated with a GIS package by subtracting the maximum elevation of the upstream drainage basin for each pixel by its local elevation. The lithology factor is averaged for each pixel's upstream contributing basin derived from an input lithology factor map. Pixel-explicit basin averaging is calculated in WBMsed by

$$\vec{F_n} = \frac{\sum_{i=1}^{n} F_i P_i}{A_n}, \tag{8}$$

where $\vec{F}$ is the spatially averaged model parameter for a pixel with n number of contributing pixels, F is the value of that parameter in a contributing pixel i, P_i is that pixel area, and A is the total drainage area to pixel n.

WBMsed uses the WBMplus daily discharge ($Q_{[i]}$) predictions (the *MDDischarge.c* module) both for the Psi equation (Eqs. (7a)–(7d)) and to derive long-term average discharge ($\overline{Q}$) for each pixel (Eqs. (4a) and (4b); Fig. 1). Temporal averaging is calculated in WBMsed by

$$\overline{F_t} = \frac{\sum_{j=1}^{t} F_j}{t}, \tag{9}$$

where $\overline{F}$ is a temporally average model parameter after t number of time steps (days in this model) and F is the parameter value in time step j.

The model uses temperature time-series maps (describe pixel-scale variation in temperature) to simulate basin average

temperature (T; Eqs. (4a) and (4b)). WBMsed averages these input in space and time (Eqs. (8) and (9), respectively).

A glacier cover input map is applied in WBMsed to set the glacial erosion parameter (I; Eq. (5)). For the human soil erosion factor (E_h) WBMsed uses population time-series maps and a Gross National Income (GNI) input map. WBMsed averages these two parameters in space (Eq. (8)) and updates them during the simulations.

The reservoir sediment trapping parameter (T_E) is based on Kettner and Syvitski (2008; HydroTrend v.3.0 model) and described in detail there. WBMsed uses reservoir capacity time series input maps for large reservoirs and the WBMplus small reservoirs capacity calculations (the *MDSmallReservoirCap.c* module) to determine trapping efficiencies. The trapping parameter is spatially averaged and temporally updated during the simulation.

The two long-term average parameters (discharge and temperature) are calculated in a separate module (*MDBQARTprepro-cess.c*) to reduce the model runtime. This module temporally sums discharge and temperature in each pixel and exports these to two corresponding output maps. These two maps are then used as input in the main module (*MDSedimentFlux.c*) to calculate long-term average discharge and temperature ($\overline{Q}$ and T, respectively; Eqs. (4a) and (4b)). This approach allows the user to calculate these two parameters only once for each simulated domain rather than resimulate them in each simulation.

3. Validation

Model predictions are evaluated by:

(1) A correlation analysis between predicted (by WBMsed and BQART) and observed (M&F05 database) long-term average sediment loads obtained at 95 coastal river mouths. This analysis is primarily intended to test the distributed implementation of BQART in WBMsed against its point-scale origin (Syvitski and Milliman, 2007). For this validation we use a global-scale simulation at a 0.5° spatial resolution.
(2) A comparison between predicted and observed daily sediment fluxes (1997–2007) at 11 USGS hydrological stations across the United States. This comparison will help evaluate the WBMsed predictions in both space and time. For this validation we use a simulation of continental North America at a 0.1° spatial resolution.

3.1. Simulation input datasets

Below we provide a summary of the datasets used for the simulations presented. The datasets source name (e.g., NCEP), listed below, corresponds to its name on the CSDMS High Performance Computer Cluster (HPCC) server. All the datasets below (and more) are available to registered users of the CSDMS HPCC. Registration is free at http://csdms.colorado.edu.

The following datasets were compiled by the University of New Hampshire and City College of New York as part of the WBMplus development (described in more detail in Wisser et al. (2010a,b)):

(1) Air temperature—NCEP—daily time steps, 1948–2009, 1° spatial resolution (Kalnay et al., 1996; Kistler et al., 2001);
(2) Precipitation—GPCCfull—monthly time steps (with supplementary daily fraction dataset), 1901–2007, 0.5° spatial resolution.
(3) Flow Network—PotSTNv602 for global and PotSTNv120 for North America simulations—static, 0.5° and 0.1° spatial resolution, respectively (Vörösmarty et al., 2000).

(4) Soil parameters—WBM-FAO soil map[1] combined terrestrial ecosystem model vegetation (Melillo et al., 1993) and croplands (Ramankutty and Foley, 1999) with WBM parameterization (Vörösmarty et al., 1998)—static, 0.1° spatial resolution.
(5) Growing season start—computed-CRU+FAO—computed from CRU air temperature using FAO guidelines (Wisser et al., 2008)—static, 0.5° spatial resolution.
(6) Irrigation area fraction—GMIA—from Global Map of Irrigated Areas[2] obtained from International Water Management Institute (IWMI) that was extended to be a time series data set by Wisser et al. (2008)—annual time steps, 1900–2009, 0.1° spatial resolution.
(7) Irrigation intensity and efficiency—Dwisser—assigned to the irrigation area fraction according to FAO guidelines (Allen et al., 1998)—static, 0.5° spatial resolution.
(8) Reservoir capacity—UNH661—based on Vörösmarty et al. (1997a, b)—annual time step, 1900–2008, 0.1° spatial resolution.
(9) Small reservoir storage fraction—GMIAderived—derived form GMIA (Wisser et al., 2010b)—annual time step, 1901–2008, 0.1° spatial resolution.
(10) Crop fraction—SAGE—from Ramankutty and Foley (1999)—static, 0.5° spatial resolution.
(11) Ice Cover—ICE5Gv102—static, 0.5° spatial resolution.
(12) Population—HYDE-CIESIN—annual time steps, 1960–2015, 0.5° spatial resolution.
    The following datasets were newly complied for the WBMsed model:
(13) Maximum relief (R)—the difference between the maximum (hinterland) and minimum (outlet) elevation for each pixel. Minimum elevation is the local elevation derived from a DEM (ETOPO1). Maximum elevation for each pixel is determined with the PsHIC (pixel-scale hypsometric integral calculator; available at: ⟨http://csdms.colorado.edu/wiki/Model:PsHIC⟩) model (Cohen et al., 2008b) using the PotSTN network for flow direction and ETOPO1 for elevation—static, 0.1° spatial resolution.
(14) Lithology factor (L)—Syvitski and Milliman (2007) converted the Dürr et al. (2005) global lithology map to a lithology factor map—static, 0.1° spatial resolution.
(15) GNI—a global country-scale Gross National Income map for the year 2000 obtained from the World Bank.

3.2. Global long-term average sediment loads

The implementation of the BQART model in WBMsed requires a more spatially and temporally explicit calculation of the model parameters compared to its point-scale origin (i.e., Syvitski and Milliman, 2007; Kettner and Syvitski, 2008; see Section 2.4). In this validation procedure we test how this spatially explicit calculation has affected the model predictions by comparing WBMsed long-term average sediment loads ($\overline{Qs}$; Eqs. (4a) and (4b)) to the original BQART results as well as to observed sediment loads from the M&F05 database (Syvitski and Milliman, 2007). Syvitski and Milliman (2007) used the M&F05 database to test the BQART model and found a very strong correlation ($R^2 = 0.97$) between BQART-predicted and M&F05-listed sediment loads. For this study 95 out of the 488 rivers of M&F05 were selected based on: (1) drainage basin size larger than 2500 km² (pixel size limitation) and (2) rivers that have a

---

[1] http://www.fao.org/ag/agl/agll/wrb/soilres.stm.
[2] http://www.iwmigiam.org/info/main/aboutGMLULC.asp.

discrepancy of less than 10% between M&F05-listed and WBMsed-calculated drainage area (used as indication of geographic fit).

Fig. 2 shows a global map of WBMsed-predicted long-term average (1948–2007) suspended sediment load. Overlaying this map are the WBMsed-predicted, BQART-calculated, and M&F05-observed long-term average suspended sediment loads (at a logarithmic scale) for the 95 rivers at their outlet (the M&F05 subset). Fig. 3 is a corresponding sediment yield map calculated by dividing sediment load by upstream contributing area and Fig. 4 is a long-term average water discharge map. Overall the WBMsed predictions correspond well to observed sediment loads. Three regions are uniformly underpredicted by WBMsed: East Asia, the Mediterranean basin, and northwestern North America. Other poorly predicted rivers are sporadically distributed around the globe (e.g., the Volta River, West Africa, and the Penner River, east India). The BQART predictions better match the M&F05-listed

observed sediment loads at almost all of the 95 river mouths (two clear exceptions are the Yenisei and San Francisco rivers in north Asia and eastern South America, respectively).

Correlation analysis between the two models and observed sediment loads (Fig. 5) quantifies the above observations. WBMsed generally underpredict long-term suspended sediment load with a moderate correlation ($R^2=0.66$) to observations (Fig. 5(a)). The correlations between WBMsed and BQART predictions are stronger with a R^2 of 0.77 (Fig. 5(b)). BQART yields a very strong correlation to observed long-term loads ($R^2=0.96$; Fig. 5(c)), which corresponds to the results of Syvitski and Milliman (2007) with the whole M&F05 database.

A detailed correlation analysis between WBMsed and BQART predictions is determined to investigate the sources of the bias (Table 1). The results indicate that the B parameter (Eqs. (4a), (4b), and (5)) is the main source of bias between the models. The low correlation in the B parameter ($R^2=0.1$) can be explained by
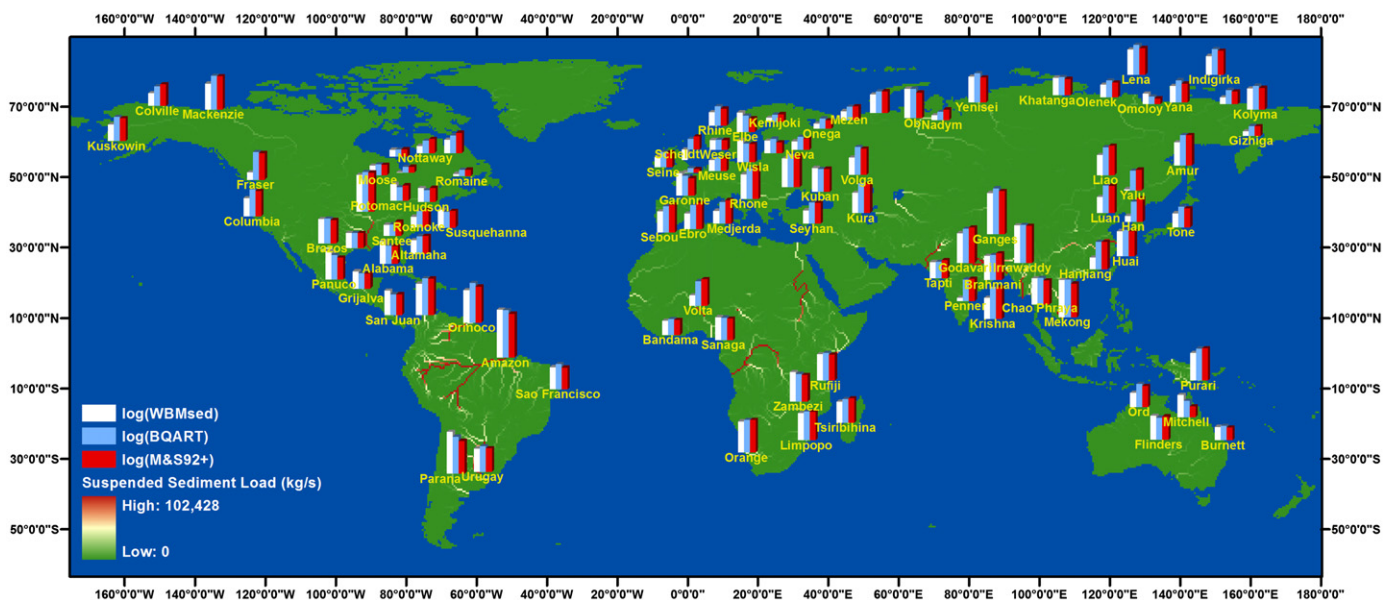

Fig. 2. Long-term (1948–2007) average suspended sediment load (kg s^{-1}) map (0.5° spatial resolution), overlaying with point predictions/observations (on a logarithmic scale) by WBMsed, BQART, and M&F05 for 95 selected river-mouth locations.
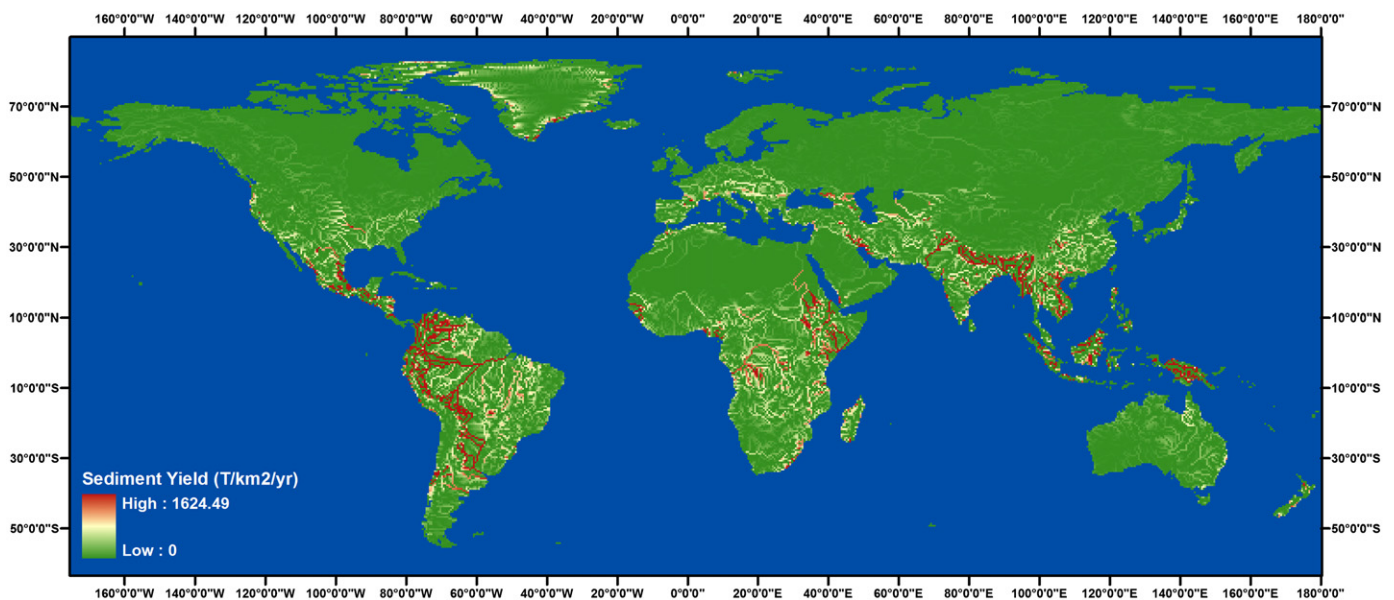

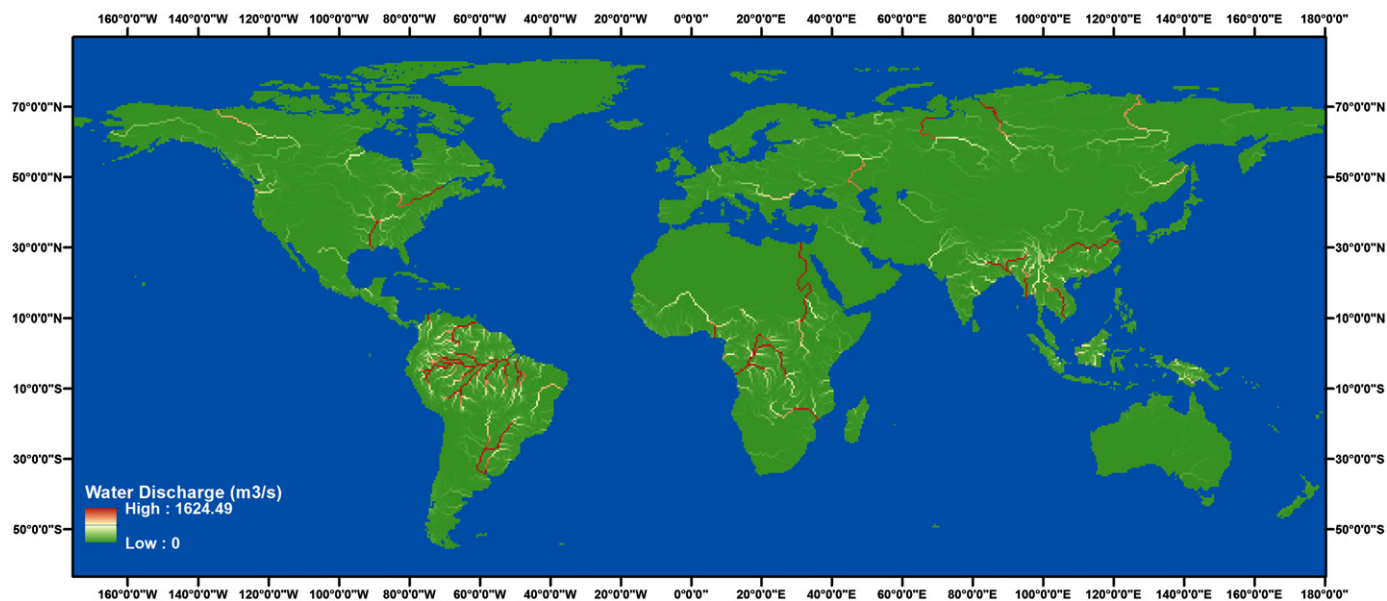**Fig. 3.** Long-term (1948–2007) average suspended sediment yield (T km^2 year^{-1}) map (0.5° spatial resolution).

Fig. 4. Long-term (1948–2007) average water discharge ($m^3 s^{-1}$) map (0.5° spatial resolution).

Table 1
Correlation between parameters of Eqs. (4a), (4b), and (5) with the original BQART model calculations (Syvitski and Milliman, 2007) and the WBMsed predictions for 95 rivers at the river mouth (subset of the M&F05 global river database).

Parameter	R^2
Q (discharge)	0.70
Area	0.99
Relief	0.84
Temperature	0.94
B	0.10
Lithology	0.22
T_e (trapping)	0.04
E_h (human)	0.11

the different ways in which its factors (ice cover, lithology factor, trapping coefficient, and human influence; Eq. (5)) are determined in the two models. The lithology factor (L) was approximated in BQART (Syvitski and Milliman, 2007) for each river basin while in WBMsed it is explicitly calculated for each pixel based on its contributing area. The trapping coefficient (T_E) in BQART was evaluated for each basin based on a global dam map while in WBMsed we use the spatially and temporally dynamic calculation of reservoir capacity of the WBMplus model. The human influence parameter (E_h) is a somewhat arbitrary threshold between population density and GNI. In Syvitski and Milliman (2007) this parameter is fixed in time and basin-averaged (a basin is either erosive ($E_h=2$), less erosive ($E_h=0.3$), or neutral ($E_h=1$)) while in WBMsed it is spatially explicit (calculated for each pixel and averaged based on its contributing area) and temporally dynamic (time varying population data). The underpredictions in eastern Asia seem to relate to this factor as the significant increase in China's (and other south-east Asian countries) GNI in the last decade has moved this part of the world from an erosive region in BQART (high population density and low GNI) to a largely neutral region (high population density with moderate GNI).

Average water discharge ($\overline{Q}$; Eqs. (4a) and (4b)) is moderately correlated ($R^2=0.70$; Table 1). This moderate correlation between long-term average discharge prediction by the WBMplus model and M&F05-listed values (used in BQART in Syvitski and Milliman, 2007) can potentially be a reliable description of the model's discharge prediction accuracy. However, this also highlights the embedded uncertainties in the M&F05 dataset. M&F05 is, by far,

the best and most comprehensive global river database. However the dataset is inevitably based on multiple sources with varying measuring (or estimation) techniques and time spans resulting in a potentially considerable degree of uncertainties. This is particularly true for long-term average values as most rivers have often only limited, short-term observations publically available.

3.3. North America daily suspended sediment fluxes

WBMsed daily sediment and discharge flux predictions are compared to observations from 11 USGS hydrological stations (Table 2) across the continental United States (Fig. 6). The hydrological stations were selected by querying the USGS "Water Data for the Nation" website (http://waterdata.usgs.gov) for those with continued daily measurements between 1997 and 2007 and a drainage area larger than 100 km^2 (pixel size limitations for this regional simulation). Although most stations are concentrated in the central part of the United States, they do represent a wide range of hydrologic and climatic regions. Seven stations are located in the Mississippi River basin ranging from an upstream station draining 190 km^2 (Yahara River at Windsor, WI) to a lower Mississippi station draining approximately 3×10^6 km^2 (Tarbert Landing, MS). The northernmost station is located at 46.8° latitude (Clark Fork, MT) and the southernmost at 37.2° latitude (Tarbert Landing, MS).

For this comparison a daily WBMsed simulation of North America between 1997 and 2007 with a spatial resolution of 0.1° is used. When averaged, the 11 years daily suspended sediment and water discharge predictions strongly correlate to observed loads (Fig. 7). This shows that for these 11 locations WBMsed can accurately predict multiyear average discharge and sediment fluxes, albeit a few outliers. This is an encouraging indication of the model multiyear average prediction capabilities and its spatially distributed implementation.

As described in Section 2.3, the Psi model (Eqs. (6) and (7a)–(7d)) is capable of capturing the intra- and interannual variability of natural rivers. It is not designed to accurately capture time series of daily sediment fluxes rather to represent a typical instantaneous value. The $\psi_{[i]}$ parameter includes a daily lognormal random variable that can lead to daily sediment load predictions ranging more than two orders of magnitude at the tail ends of the lognormal distribution. This implies that WBMsed can realistically predict a range of daily sediment fluxes rather than a
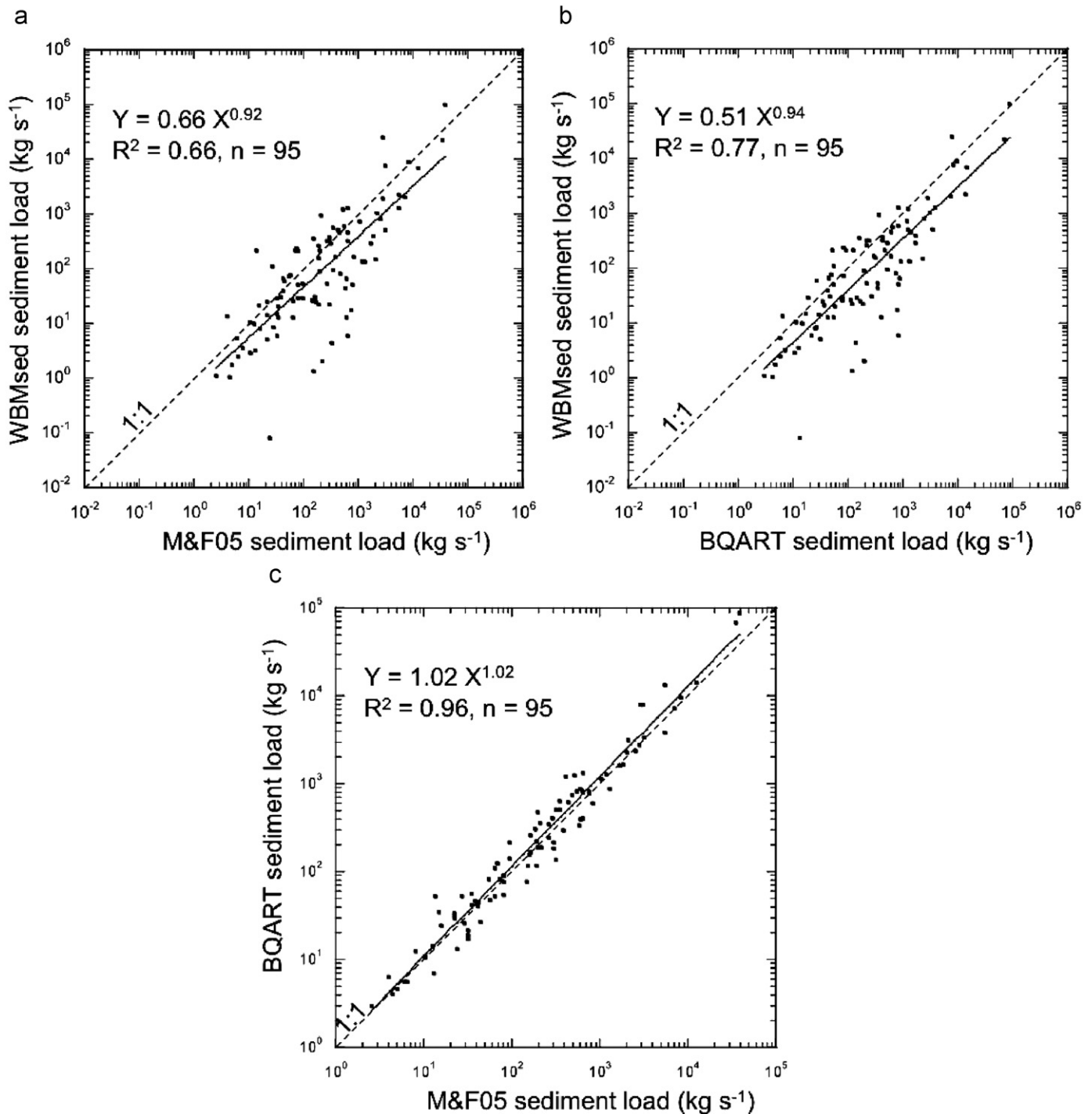
Fig. 5. Comparison of long-term (1948–2007) average sediment load for 95 rivers at the river mouth (M&F05 subset) for (a) WBMsed-predicted and M&F05-observed; (b) WBMsed-predicted and BQART-calculated; and (c) BQART-calculated and M&F05-observed.

single value. Fig. 8 demonstrates this by plotting the extreme range in daily sediment flux predictions as a function of the Psi daily random variable for one station (no. 3, Mississippi River at Chester, IL; Fig. 6 and Table 2). The time series in Fig. 8 compare the observed and predicted daily sediment flux (blue and red dots, respectively) and show the model daily sediment prediction range (gray error bars).

Fig. 9 shows the daily discharge and sediment flux-time series for all 11 stations. For clarity it does not include the model sediment flux prediction range demonstrated in Fig. 8. Overall WBMsed captures the interannual and intraannual trends in water discharge and sediment fluxes. Daily sediment predictions show a considerably higher degree of scatter compared to observations. The model tends to considerably over- and under-predict sediment flux in high and low discharge periods, respectively. Daily sediment flux results of station nos. 8 and 11 (Fig. 9) should be considered with some reservation as they drain relatively small areas, generating average annual water discharges below 30 $m^3 s^{-1}$, well below the validated minimum water discharge that was used to establish the BQART long-term sediment relation (Syvitski and Milliman, 2007). These smaller streams inevitably represent different sediment erosion,

deposition, and transport processes, which are not entirely captured with BQART. This might be the reason why for station number 11 the sediment is actually less underpredicted than most other stations. Fig. 9 shows that sediment flux over- and underpredictions are strongly driven by water discharge over- and underpredictions, respectively.

Codependence between discharge and sediment predictions is also evident from the regression analysis between observed and predicted daily, monthly, and yearly averages summarized in Table 3. Stations with below average R^2 for discharge (0.38 for daily) result in below average R^2 for sediment as well (0.29 for daily). In addition, stations draining small contributing area ($> 69,000$ km^2; Table 2) yield a below average R^2 while stations with large contributing area yield a much better fit between observed and predicted discharge and sediment (except for station no. 5).

Quality of fit between observed and predicted discharge and sediment is considerably higher for monthly and yearly averages (average R^2 of 0.57 and 0.54 for monthly average for discharge and sediment, respectively) relative to daily predictions (Table 3), particularly for stations with larger contributing areas.

4. Discussion

The first validation procedure (Section 3.2) analyzes the extent to which WBMsed explicit parameter calculations have affected the model's predictions compared to the original point-scale BQART calculation. The results show that WBMsed predictions are moderately correlated to BQART-calculated and M&F05-listed sediment loads (R^2 of 0.77 and 0.66, respectively; Fig. 3). The model's physical parameters (area, relief and temperature) are well correlated (R^2 of 0.99, 0.84, and 0.94, respectively; Table 1) to

Table 2
Characteristics of 11 USGS hydrological stations (Fig. 6) used to validate WBMsed daily sediment and discharge fluxes.

Map ID	Name	USGS site number	USGS site coordinates lat/long (dd)	WBMsed point coordinates lat/long (dd)	USGS site drainage area (km^2)	WBMsed point drainage area (km^2)
1	Mississippi River at Tarbert Landing, MS	7295100	31.00/91.62	31.05/91.65	2913 477	3206 630
2	Mississippi River at Thebes, IL	7022000	37.21/89.46	37.25/89.55	1847 179	1841 230
3	Mississippi River at Chester, IL	7020500	37.90/89.83	37.85/89.85	1835 265	1828 800
4	Mississippi River at St. Louis, MO	7010000	38.62/90.17	38.65/90.15	1805 221	1798 620
5	Missouri River at Nebraska City, NE	6807000	40.68/95.84	40.65/95.85	1061 895	1056 940
6	Illinois River at Valley City, IL	5586100	39.70/90.64	39.75/90.65	69264	69450
7	Skunk River at Augusta, IA	5474000	40.75/91.27	40.75/91.25	11168	11202
8	Yahara River at Windsor, WI	5427718	43.20/89.35	43.25/89.35	190	179
9	San Joaquin River near Vernalis, CA	11303500	37.67/121.26	37.65/121.25	35058	22772
10	Sacramento River at Freeport, CA	11447650	38.45/121.50	38.45/121.55	Not listed	69457
11	Clark Fork at Turah Bridge near Bonner, MT	12334550	46.82/113.81	46.85/113.85	9430	9471

The stations name, USGS number, USGS coordinates, and USGS drainage area are obtained from the USGS "Water Data for the Nation" (http://waterdata.usgs.gov).
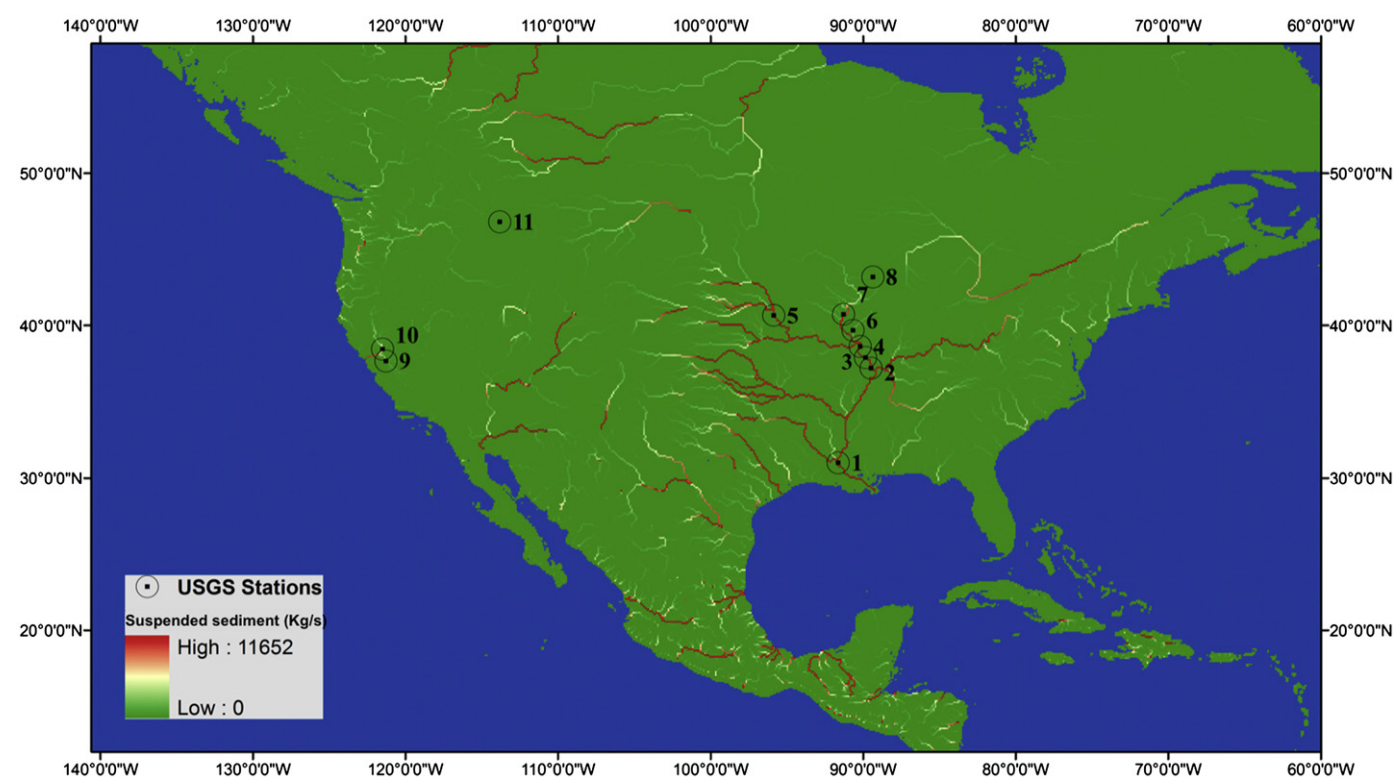

Fig. 6. WBMsed-predicted average suspended sediment load for 2007 (0.1° spatial resolution) over continental North America and the selected 11 USGS hydrological stations used for validation (Table 2).
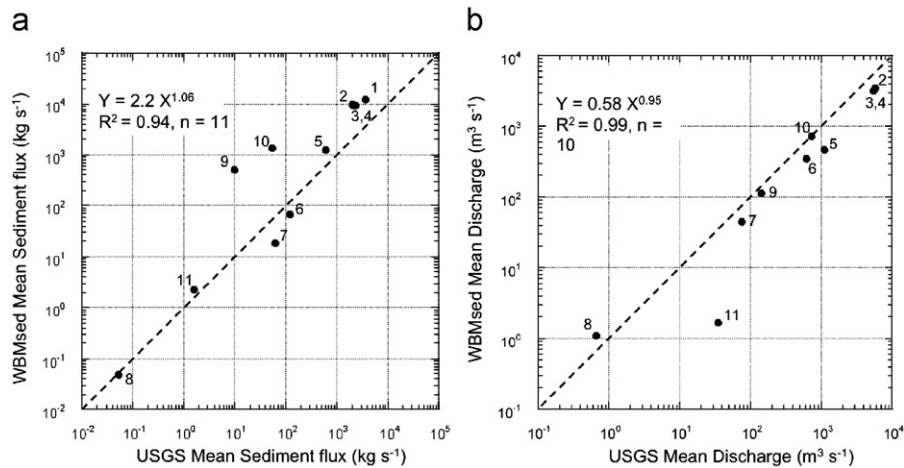
Fig. 7. Comparison between WBMsed-predicted and USGS-observed mean (a) suspended sediment and (b) water discharge between 1997 and 2007. The numbers correspond to the USGS station ID in Table 2 and Fig. 6. Dotted line represents the 1 to 1 line.

their original values in BQART (Syvitski and Milliman, 2007), while the more qualitative or temporally dynamic parameters (lithology factor, trapping efficiency and human erosivity) are poorly correlated (R^2 of 0.22, 0.04, and 0.11, respectively). Even though a more explicit calculation of the model parameters is typically expected to improve its accuracy, the empiricism of the BQART equations will inevitably better correspond to the dataset used to compile it. We therefore expect that a recalibration of the BQART equation based on the explicit WBMsed parameter calculations will improve the fit between predicted and observed long-term average sediment loads.

The second validation procedure (Section 3.3) analyzes WBMsed temporal and spatial capabilities by comparing daily discharge simulations and sediment flux predictions against measured fluxes across the continental United States (11 USGS stations). Strong correlations between 11 years average predicted and observed sediment and discharge flux (Fig. 7) suggest that WBMsed can well predict multiyearly average sediment loads. It also indicates that it can well predict inland spatially distributed suspended sediment loads, similar to those found by Kettner et al. (2010). The correlation between observed and predicted average sediment loads is much stronger in this analysis relative to the global-scale comparison against the M&F05 dataset (R^2 of 0.97 compared to 0.66). Even though we only compare 11 locations for this analysis with a smaller geographic spread, the observed data in this case is much more robust as the M&F05 database is based on a wide variety of sources with varying measurement durations. The USGS stations used are also independent of the BQART calibration of Syvitski and Milliman (2007). This increases our confidence in the explicit implementation of the BQART equations in WBMsed and suggests that a recalibration of the BQART equation may not be required for this kind of spatially explicit application (as suggested in first river-mouth analysis).

WBMsed was able to capture the interannual and intraannual fluctuations in water discharge and suspended sediment fluxes (Fig. 9 and Table 3) but considerably over- and underpredicts daily sediment fluxes during peak and low discharge periods, respectively. We identify two possible causes of these over and underpredictions: (1) the Psi model capabilities (Fig. 8), and (2) the model's water discharge predictions. We test these sources of bias by calculating daily sediment flux for station no. 3 and no. 9 (Fig. 6 and Table 2), using USGS-observed water discharge (Fig. 9(3) and (9)) for $Q_{[i]}$ in Eq. (6). Using observed, rather than model-predicted, water discharge eliminates most of the model underpredictions and much of its overpredictions (Fig. 10). It,
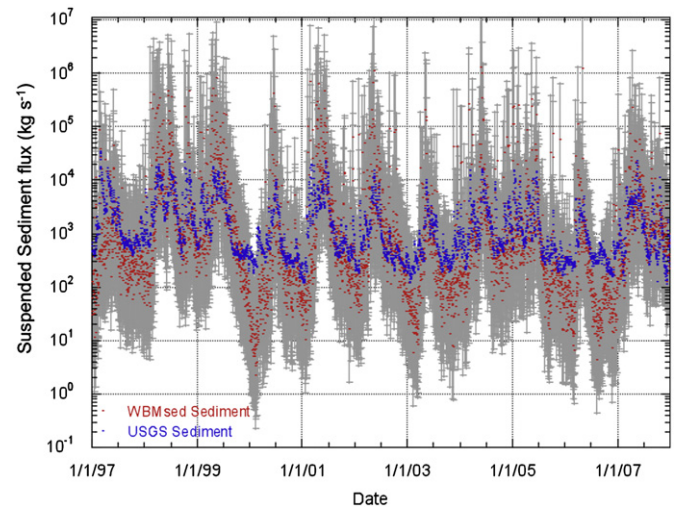

Fig. 8. Daily sediment flux time series for station no. 3 (Mississippi River at Chester, IL; Fig. 6 and Table 2). The gray error bars represent the maximum rage of the Psi daily predictions as a function of it lognormal random parameter (Eqs. (6) and (7a)–(7d)). (For interpretation of the references to color in this figure, the reader is referred to the web version of this article.)

however, still shows a considerable degree of scatter compared to observed daily fluxes. The correlation between observed and predicted sediment flux improves dramatically for both stations (3b and 9b in Table 3) from R^2 of 0.39 to 0.68 in station no. 3 and from 0.12 to 0.67 in station no. 9 for daily sediment fluxes. This shows that improving the model daily water discharge predictions will considerably improve its suspended sediment flux predictions; however, the Psi model still generates a considerable degree of scatter.

5. Conclusions

Results of the two validation procedures (long-term average and daily comparison) lead us to conclude that WBMsed can well predict multiyearly average sediment flux over diverse geographical settings. This shows that the spatially explicit implementation of the BQART model in WBMsed (assuming that each pixel is an outlet of its upstream contributing area) is robust and that WBMsed can be applied to study long-term sediment trends.
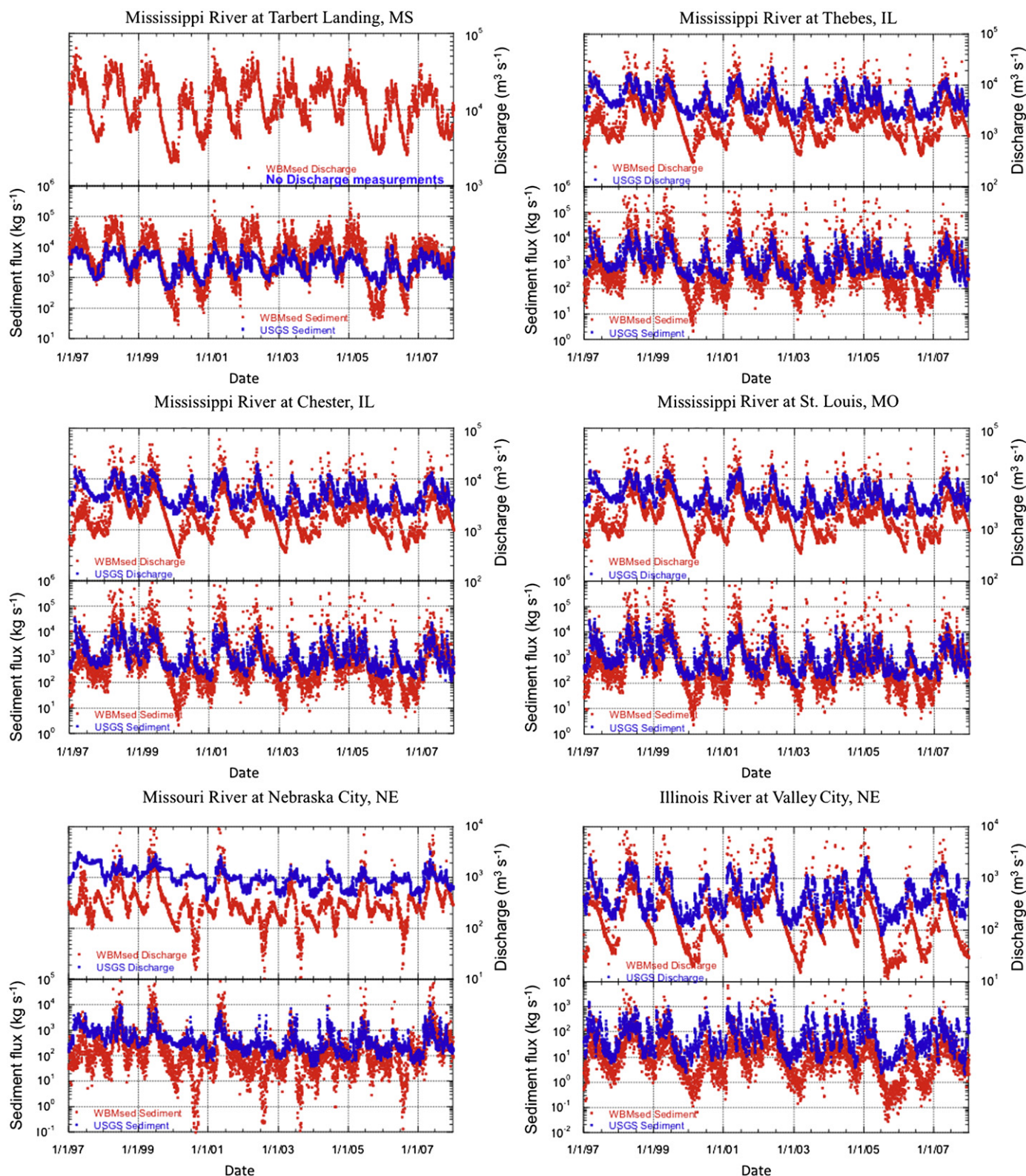
Fig. 9. Eleven years (1997–2007) daily time series of water discharge (top plots) and suspended sediment (bottom plots) fluxes for each of the 11 USGS hydrological stations (title numbering corresponds to Fig. 5 and Table 2). USGS-measured fluxes are displayed in blue and WBMsed-predicted in red. In some plots a small portion (<1%) of predicted daily fluxes are not displayed in favor of a smaller plotting range on the *y*-axis. No discharge observations were available for station no. 1. (For interpretation of the references to color in this figure legend, the reader is referred to the web version of this article.)

Analysis of daily sediment predictions led us to conclude that the main source of bias is the simulated water discharges. When observed water discharge was used as input, sediment predictions were improved considerably. However, even with observed discharge WBMsed daily sediment predictions are scattered. This led us to conclude that the Psi modeling approach
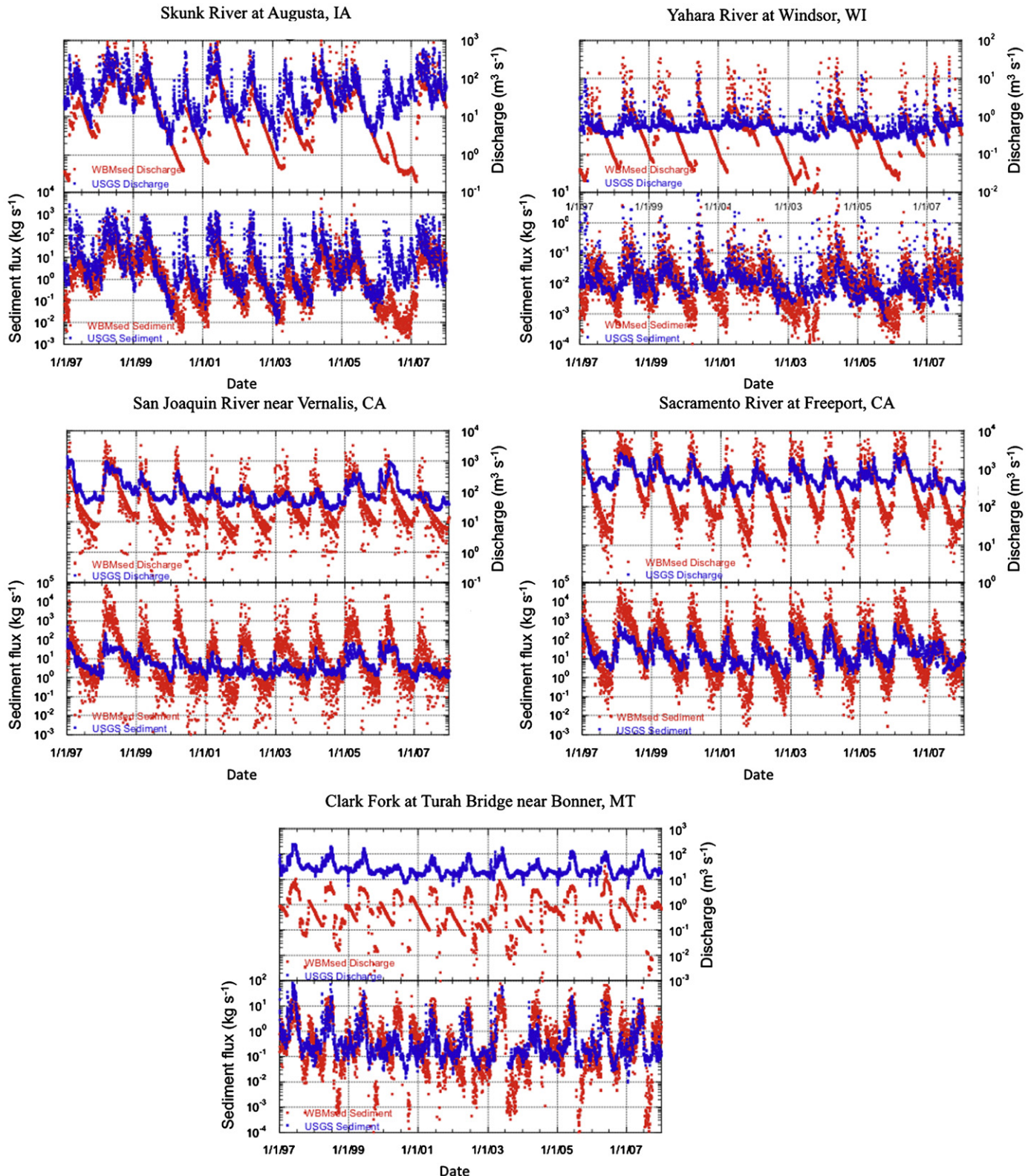
Fig. 9. (*continued*)

(used in WBMsed to extract short-term sediment fluxes from long-term average fluxes) might be less suitable for daily sediment predictions.

The results also indicate that WBMsed predictions are less reliable for smaller catchments (below 69,000 km^2).

These limitations can be addressed by first improving WBMsed water discharge predictions and later by revisiting the Psi approach. We believe that extreme over- and underpredictions of water discharge can be addressed by introducing a flood plain reservoir component. This approach, currently being tested, will

Table 3

Regression analysis results (equations and R^2) for daily, monthly, and yearly predicted versus observed water discharge and sediment flux in 11 USGS hydrological stations.

Map ID	Daily discharge		Daily sediment		Monthly discharge		Monthly sediment		Yearly discharge		Yearly sediment	
	Eq.	R^2	Eq.	R^2	Eq.	R^2	Eq.	R^2	Eq.	R^2	Eq.	R^2
1			$0.006x^{1.70}$	0.64			$0.002x^{1.85}$	0.76			$3.801x-1692.5$	0.48
2	$0.079x^{1.19}$	0.48	$0.29x^{1.11}$	0.36	$0.0098x^{1.45}$	0.78	$0.021x^{1.60}$	0.70	$0.908x-1859.2$	0.69	$5.808x-2095.1$	0.63
3	$0.062x^{1.22}$	0.49	$0.273x^{1.11}$	0.39	$0.0077x^{1.48}$	0.78	$0.033x^{1.52}$	0.70	$0.917x-1786.3$	0.67	$4.314x-281.1$	0.58
3b			$7.490x^{0.90}$	0.68			$7.062x^{0.92}$	0.90			$3.561x+1376.9$	0.86
4	$0.058x^{1.22}$	0.51	$0.516x^{1.03}$	0.38	$0.0077x^{1.48}$	0.78	$0.058x^{1.46}$	0.70	$0.901x-1701$	0.68	$4.389x+8.571$	0.60
5	$0.548x^{0.91}$	0.18	$0.375x^{0.96}$	0.21	$0.2305x^{1.04}$	0.26	$0.075x^{1.29}$	0.42	$0.238x+204.58$	0.12	$1.704x+206.96$	0.14
6	$0.209x^{1.07}$	0.48	$0.367x^{0.82}$	0.35	$0.0369x^{1.38}$	0.70	$0.098x^{1.24}$	0.69	$1.064x-320.8$	0.77	$1.177x-74.324$	0.67
7	$0.498x^{0.83}$	0.30	$0.468x^{0.57}$	0.30	$0.2097x^{1.11}$	0.47	$0.380x^{0.78}$	0.48	$0.848x-18.81$	0.88	$0.331x-1.3172$	0.60
8	$0.783x^{1.37}$	0.18	$0.128x^{0.53}$	0.14	$1.3738x^{2.21}$	0.34	$0.228x^{0.62}$	0.28	$3.887x-1.463$	0.53	$0.577x+0.016$	0.52
9	$0.005x^{1.62}$	0.34	$0.063x^{1.18}$	0.12	$0.1169x^{1.27}$	0.48	$0.529x^{1.97}$	0.48	$0.573x+33.297$	0.53	$70.759x-189.75$	0.57
9b			$5.015x^{1.34}$	0.67			$5.516x^{1.42}$	0.86			$45.881x-163.41$	0.88
10	$0.001x^{1.94}$	0.53	$0.204x^{1.61}$	0.50	$0.0002x^{2.20}$	0.66	$0.094x^{2.02}$	0.71	$1.544x-368.85$	0.86	$38.109x-620.16$	0.48
11	$2E-05x^{2.85}$	0.25	$0.562x^{1.58}$	0.17	$0.0003x^{2.20}$	0.45	$0.926x^{1.03}$	0.28	$0.015x+0.859$	0.23	$0.129x+2.011$	0.10

The "Map ID" corresponds to Table 2 and Fig. 6. For the daily and monthly analysis a power-law-fit equation is used (log–log linear). For the yearly analysis a linear fit equation is used as the range of the data points is less than an order of magnitude.
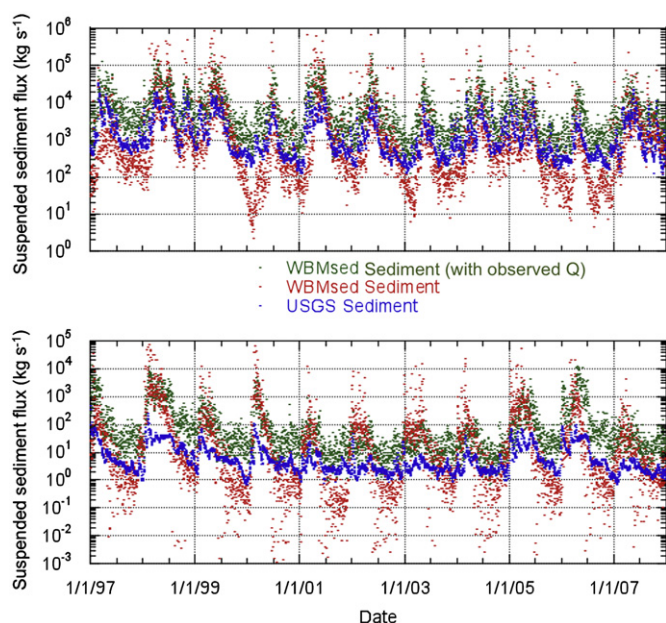

Fig. 10. Sediment flux time series for (a) station no. 3 and (b) station no. 9 (Fig. 6 and Table 2) using observed rather than simulated water discharge values (Fig. 9(3) and (9)). These plots show that improving WBMsed water discharge predictions will considerably reduce sediment flux missmatches.

store water from the river when discharge exceeds bankfull and gradually return it when water recedes. More explicit modeling of sediment cascade by a sediment-transport modeling approach will potentially improve the model's daily predictions addressing the Psi model limitations.

Acknowledgments

Appendix A. Supplementary material

Supplementary data associated with this article can be found in the online version at doi:10.1016/j.cageo.2011.08.011.

References

Allen, R.G., Pereira, L.S., Raes, D., Smith, M., 1998. Crop Evapotranspiration: Guidelines for Computing Crop Water Requirements. Food and Agricultural Organization of the United Nations (FAO).

Biemans, H., Hutjes, R.W.A., Kabat, P., Strengers, B.J., Gerten, D., Rost, S., 2009. Effects of precipitation uncertainty on discharge calculations for main river basins. Journal of Hydrometeorology 10, 1011–1025.

Cohen, S., Svoray, T., Laronne, J.B., Alexandrov, Y., 2008a. Fuzzy-based dynamic soil erosion model (FuDSEM): modelling approach and preliminary evaluation. Journal of Hydrology 356, 185–198. doi:10.1016/j.jhydrol.2008.04.010.

Cohen, S., Willgoose, G., Hancock, G., 2008b. A methodology for calculating the spatial distribution of the area-slope equation and the hypsometric integral within a catchment. Journal of Geophysical Research-Earth Surface 113, F03027. doi:10.1029/2007JF000820.

Cohen, S., Willgoose, G., Hancock, G., 2009. The mARM spatially distributed soil evolution model: a computationally efficient modeling framework and analysis of hillslope soil surface organization. Journal of Geophysical Research 114, F03001. doi:10.1029/2008JF001214.

Cohen, S., Willgoose, G., Hancock, G., 2010. The mARM spatially distributed soil evolution model: three-dimensional model framework, and analysis of hillslope and landform responses. Journal of Geophysical Research 115, F04013. doi:10.1029/2009JF001536.

Dürr, H.H., Meybeck, M., Dürr, S.H., 2005. Lithologic composition of the Earth's continental surfaces derived from a new digital map emphasizing riverine material transfer. Global Biogeochemical Cycles 19 (4), 23.

Federer, C.A., Vörösmarty, C., Fekete, B.M., 1996. Intercomparison of methods for calculating potential evaporation in regional and global water balance models. Water Resources Research 32, 2315–2321.

Fekete, B.M., Vörösmarty, C.J., Grabs, W., 2002. High resolution fields of global runoff combining observed river discharge and simulated water balances. Global Biochemical Cycles 16, 15-1–15-6.

Fekete, B.M., Vörösmarty, C.J., Roads, J., Willmott, C., 2004. Uncertainties in precipitation and their impacts on runoff estimates. Journal of Climatology 17, 294–303.

Hamon, W.R., 1963. Computation of direct runoff amounts from storm rainfall. In: Proceedings of the Symposium on Surface Waters, IAHS Publications, vol. 63, pp. 52–62.

Kalnay, E., Kanamitsu, M., Kistler, R., Collins, W., Deaven, D., Gandin, L., Iredell, M., Saha, S., White, G., Woolen, J., Zhu, Y., Chelliah, M., Ebisuzaki, W., Higgis, W., Janowiak, J., Mo, K.C., Ropelewski, C., Wang, J., Leetmaa, A., Reynolds, R., Jenne, R., Joseph, D., 1996. The NCEP/NCAR 40-year reanalysis project. Bulletin of the American Meteorological Society 77, 437–472.

Kettner, A.J., Restrepo, J.D., Syvitski, J.P.M., 2010. A spatial simulation experiment to replicate fluvial sediment fluxes within the Magdalena River Basin, Colombia. Journal of Geology 118 (4), 363–379.

Kettner, A.J., Syvitski, J.P.M., 2008. HydroTrend v.3.0: a climate-driven hydrological transport model that simulates discharge and sediment load leaving a river system. Computers & Geosciences 34 (10), 1170–1183.

Kettner, A.J., Syvitski, J.P.M., 2009. Fluvial responses to environmental perturbations in the Northern Mediterranean since the Last Glacial Maximum. Quaternary Science Reviews 28 (23–24), 2386–2397.

Kistler, R., Kalnay, E., Collins, W., Saha, S., White, G., Woolen, J., Chelliah, M., Ebisuzaki, W., Kanamitsu, M., Kousky, V., van den Dool, H., Jenne, R., Fiorino, M., 2001. The NCEP/NCAR 50-year reanalysis: monthly means CD-ROM and documentation. Bulletin of the American Meteorological Society 82, 247–267.

McCarney-Castle, K., Voulgaris, G., Kettner, A.J., Giosan, L., 2011. Simulating fluvial fluxes in the Danube watershed: the 'Little Ice Age' versus modern day. The Holocene, 1–16. doi:10.1177/0959683611409778.

Melillo, J.M., McGuire, A.D., Kicklighter, D.W., Moore III, B., Vörösmarty, C.J., Schloss, A.L., 1993. Global climate change and terrestrial net primary production. Nature 363, 234–240.

Milliman, J.D., Syvitski, J.P.M., 1992. Geomorphic/tectonic control of sediment discharge to the ocean—the importance of small mountainous rivers. Journal of Geology 100 (5), 525–544.

Morehead, M.D., Syvitski, J.P., Hutton, E.W.H., Peckham, S.D., 2003. Modeling the temporal variability in the flux of sediment from ungauged river basins. Global and Planetary Change 39 (1–2), 95–110.

Ramankutty, N., Foley, J.A., 1999. Estimating historical changes in global land cover: croplands from 1700 to 1992. Global Biochemical Cycles 13, 997–1027.

Syvitski, J.P.M., Milliman, J.D., 2007. Geology, geography, and humans battle for dominance over the delivery of fluvial sediment to the coastal ocean. Journal of Geology 115 (1), 1–19.

Syvitski, J.P.M., Kettner, A.J., Peckham, S.D., Kao, S.-J., 2005a. Predicting the flux of sediment to the coastal zone: application to the Lanyang watershed, Northern Taiwan. Journal of Coastal Research 21, 580–587.

Syvitski, J.P.M., Vörösmarty, C.J., Kettner, A.J., Green, P., 2005b. Impact of humans on the flux of terrestrial sediment to the global coastal ocean. Science 308 (5720), 376–380.

Vörösmarty, C.J., Federer, C.A., Schloss, A.L., 1998. Potential evaporation functions compared on US watersheds: possible implications for global-scale water balance and terrestrial ecosystem modeling. Journal of Hydrology 207, 147–169.

Vörösmarty, C.J., Fekete, B.M., Meybeck, M., Lammers, R.B., 2000. Global system of rivers: its role in organizing continental land mass and defining land-to-ocean linkages. Global Biochemical Cycles 14, 599–621.

Vörösmarty, C.J., Meybeck, M., Fekete, B., Sharma, K., 1997a. The potential of neo-Castorization on sediment transport by the global network of rivers: human impact on erosion and sedimentation. IAHS 245, 261–273.

Vörösmarty, C.J., Moore III, B., Grace, A.L., Gildea, M., Melillo, J.M., Peterson, B.J., Rastetter, E.B., Steudler, P.A., 1989. Continental scale models of water balance and fluvial transport: an application to South America. Global Biochemical Cycles 3, 241–265.

Vörösmarty, C.J., Sharma, K.P., Fekete, B.M., Copeland, A.H., Holden, J., Marble, J., Lough, J.A., 1997b. The storage and aging of continental runoff in large reservoir systems of the world. Ambio 26, 210–219.

Wilkinson, S.N., Prosser, I.P., Rustomji, P., Read, A.M., 2009. Modelling and testing spatially distributed sediment budgets to relate erosion processes to sediment yields. Environmental Modelling & Software 24, 489–501.

Wisser, D., Fekete, B.M., Vörösmarty, C.J., Schumann, A.H., 2010a. Reconstructing 20th century global hydrography: a contribution to the Global Terrestrial Network–Hydrology (GTN–H). Hydrology and Earth System Sciences 14 (1), 1–24.

Wisser, D., Frolking, S., Douglas, E., Fekete, B.M., Schuman, A.H., Vörösmarty, C.J., 2010b. The significance of local water resources captured in small reservoirs for crop production—a global-scale analysis. Journal of Hydrology 384, 264–275.

Wisser, D., Frolking, S., Douglas, E.M., Fekete, B.M., Vörösmarty, C.J., Schumann, A.H., 2008. Global irrigation water demand: Variability and uncertainties arising from agricultural and climate data sets. Geophysical Research Letters, 35. doi:10.1029/2008GL035296.

Wollheim, W.M., Vörösmarty, C.J., Bouwman, A.F., Green, P., Harrison, J., Linder, E., Peterson, B.J., Seitzinger, S.P., Syvitski, J.P.M., 2008. Global N removal by freshwater aquatic systems using a spatially distributed, within-basin approach. Global Biogeochemical Cycles 22, GB2026. doi:10.1029/2007GB002963.